

# Edge Magneto-Fingerprints in Disordered Graphene Nanoribbons

Jean-Marie Poumirol<sup>1</sup>, Alessandro Cresti<sup>2</sup>, Stephan Roche<sup>3,4</sup>, Walter Escoffier<sup>1</sup>,

Michel Goiran<sup>1</sup>, Xinran Wang<sup>5</sup>, Xiaolin Li<sup>5</sup>, Hongjie Dai<sup>5</sup>, Bertrand Raquet<sup>1</sup>

<sup>1</sup>Laboratoire National des Champs Magnétiques Intenses, INSA UPS CNRS,  
UPR 3228, Université de Toulouse, 143 av. de Rangueil, 31400 Toulouse, France

<sup>2</sup>CEA, LETI, MINATEC, F38054 Grenoble, France

<sup>3</sup>CEA, INAC, SP2M, L<sub>sim</sub>, 17 avenue des Martyrs, Grenoble, France

<sup>4</sup>CIN2 (CSIC-ICN), Campus UAB, E-08193 Barcelona, Spain and

<sup>5</sup>Department of Chemistry and Laboratory of Advanced Materials,  
Stanford University Stanford, California 94305, USA

We report on (magneto)-transport experiments in chemically derived narrow graphene nanoribbons under high magnetic fields (up to 60 Tesla). Evidences of field-dependent electronic confinement features are given, and allow estimating the possible ribbon edge symmetry. Besides, the measured large positive magnetoconductance indicates a strong suppression of backscattering induced by the magnetic field. Such scenario is supported by quantum simulations which consider different types of underlying disorders (smooth edge disorder and long range Coulomb scatters).

*Introduction.*-The control of the current flow in graphene nanoribbons (GNRs) constitutes a fascinating challenge for the future of carbon-based electronic devices. The description of low energy excitations as massless Dirac fermions in graphene (resulting in large mobility at room temperature [1]), together with the possibility for bandgap engineering [2] suggest a strategy to outperform Silicon devices [3, 4]. However, the lateral size reduction goes along with a problematic decay of the charge mobility [4, 5]. Low temperature transport measurements performed at zero magnetic field on lithographically patterned GNRs unveil an ubiquitous energy gap, irrespective of the edges symmetry [2], exceeding the expected confinement gap [6, 7] and driven by disorder induced charging effects [8, 9]. Non-perfect edges are also expected to produce a significant scattering source. Drastic consequences on the electronic transport have been theoretical anticipated with the formation of a mobility gap, even in the presence of an ultra-smooth edge roughness [10]. Other sources of disorder like bulk vacancies [11], charge trapped in the oxide [7, 9], or structural deformations (ripples) [12] are also believed to significantly alter the conductance, although the dominant scattering source remains debated, and seems to be sample dependent. In that perspective, experimental works on narrow GNRs remain sorely lacking.

This Letter presents compelling evidences of the 1D transport character in a 11nm wide GNR, and the possibility of tuning backscattering effects by means of an external magnetic field. Bandstructure calculations allow some assignment of the measured gate-dependent conductance modulations to the underlying van Hove singularities, and hence some estimation of the likely ribbon edge symmetry. The application of perpendicular high magnetic field further induces a marked enhancement of the conductance, irrespective of the applied gate voltage and in large contrast to the magnetofingerprints of graphene flakes [13]. Close to the charge neutrality

point, the measured large positive magnetoconductance (MC) is attributed to the formation of the first Landau state, responsible for the closing of the energy gap and of a marked reduction of backscattering processes. Landauer-Büttiker conductance simulations convincingly support the scenario of an entangled interplay between the magnetic bands formation and a disorder-induced interband scattering suppression. Both edge disorder and long range coulomb scatters yield similar conclusions.

*Transport measurements.*-Experiments are carried out on the first generation of chemically derived GNRs with smooth edges [14] deposited on Si/SiO<sub>2</sub>(500nm) wafer and connected to Pd-electrodes distanced by 270nm. The electrostatic doping is monitored by a back-gate voltage. In the following, we focus on a 11nm wide GNR for which the first Landau orbit of radius  $l_B = \sqrt{\hbar/eB}$  reaches the ribbon width of our GNR sample at 30T. Complementary measurements on larger GNR, here 90nm, are briefly discussed to emphasize the effect of the electronic confinement on the magnetoconductance.

Figure 1 (inset) shows the gate voltage dependent conductance of the 11nm wide GNR under 50mV bias voltage ( $V_b$ ), and at various temperatures (from 169K down to 20K). The V-shape curves are typical for a semiconducting ribbon [8]. The conductance at the CNP measured at  $V_b = 1mV$  follows a thermally activated behaviour down to 50K. Interestingly, a detailed analysis of the  $G(V_g)$  curves at 80K and below unveils reproducible modulations superimposed to the overall increase of the conductance versus gate voltage (Fig.1, main frame). These structures evolve to pronounced conductance drops for low bias measurements (blue curve obtained at 1mV). We assign such conductance profile to the presence of van Hove singularities (vHs), responsible for the enhancement of the backscattering in the diffusive regime. To validate such scenario, extensive tight-binding bandstructures calculations are performed on a set of ribbons symmetries with varying widths [15]. Calculations include

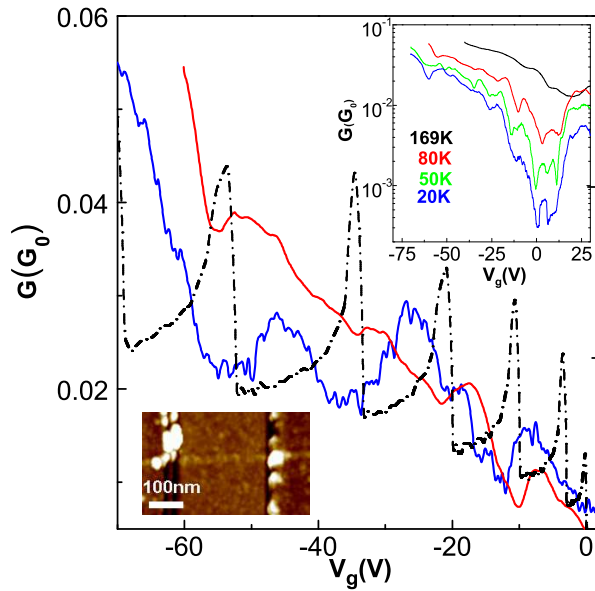


FIG. 1: (color online) Conductance versus  $V_g$  at 80K measured on the narrow GNR (width  $\simeq 11$ nm) and for two  $V_b$ , 50mV and 1mV (respectively red and blue curves). The density of states of a 90-aGNR is superimposed (dashed curve). Top inset:  $G(V_g)$  at various temperatures for a wider gate voltage range. Bottom inset: AFM image of the measured GNR device.

zigzag (zGNR) and armchair GNR (aGNR) of three types  $N=3m$ ,  $3m+1$  and  $3m+2$ ,  $N$  being the number of dimer lines. The  $N$  values are chosen to explore the full range of the ribbon sample width dispersion (here  $11 \pm 1.5$ nm), as evaluated by careful AFM analysis. Figure 1 also shows the density of states  $\rho(V_g)$  (dotted-dashed curve) for the armchair configuration of type  $3m$  with  $N = 90$  corresponding to a nominal width of 10.947nm, which turns out to be the most likely ribbon geometry obtained by the theoretical analysis [15]. Indeed, without any free parameters, a convincing agreement is observed between the local minima of conductance and the theoretical sequence of vHs's onsets. Such correspondence is not achieved at all for zGNR and other  $3m+1$  and  $3m+2$  types of aGNR [15]. Note that other  $N$  values, multiple of 3, from 87 to 93, well below the experimental width uncertainty, also lead to a satisfactory agreement. The bands arrangement undergoes a scaling of the order of 6%, which cannot be discriminated on the  $G(V_g)$  curves. We conclude that the conductance exhibits 1D subbands fingerprints consistent with an armchair arrangement of the carbon atoms at the edges with  $3m$  dimer lines, around  $90 \pm 3$ , along its width.

*Magnetoconductance behavior.*—The application of a transverse magnetic field on the 11nm wide GNR drastically increases its conductance by more than 50% at 80K and by more than one decade at 20K (Fig.2-left panel). The gain of transmission is further modulated by the electrostatic doping in a complex but very re-

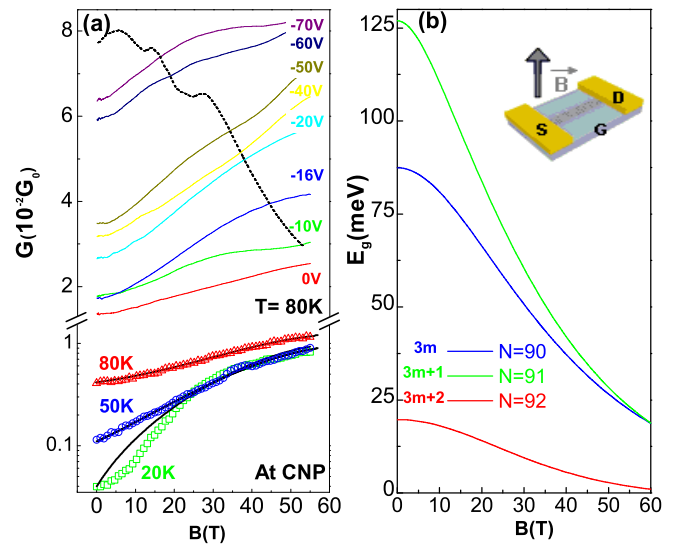


FIG. 2: (color online) (a) Left panel: Magnetoconductance at 80K for the narrow ribbon, and various gate voltages (top); and at 80K, 50K, 20K for  $V_g = 0$  (curves with symbols: measurements; solid lines : simulated data). The MC for a larger width GNR (90nm) is also shown (dashed curve). (b) Right panel: Computed field-dependent energy gaps for three different types of aGNR. Inset: Schematic of the GNR device.

producibile manner. One notes that the MC remains of large amplitude, even when several subbands are involved in conduction. Conversely, for a 90nm wide GNR (Fig.2a, black dashed curve) and generally speaking for graphene flakes [16], only the very low magnetic field MC is slightly positive and results from a weak localization regime. At larger field, the conductance of large width GNR is strongly reduced, following the two-fluid model at the CNP in a diffusive regime [17] and further exhibits a step-like decrease in the quantum regime, unveiling the graphene Landau Levels (LL) [18] and the reduction of the number of available channels at the edges [19]. In the following, we bring evidence that the large *positive* MC and its energy dependence obtained for the narrow GNR result from a subtle interplay between the specific magnetic bandstructures and the field induced reduction of disorder-driven backscattering.

The magnetic field dependent bandstructure calculations reveal that the 1D subbands of the GNR evolve to the graphene LL above 30T, once the magnetic confinement gradually overcomes the electronic one [15]. At the CNP, the onset of the zero-energy LL induces a closing of the energy bandgap of the GNR. In Fig.2b the simulated magnetic field dependence of the energy gaps for the three types of aGNR are reported. Assuming a flat band model at the CNP, the magnetic-field dependence of the ribbon energy gaps  $E_g(B)$  will modulate the thermally activated regime, in which the magnetoconductance is expressed as  $\Delta G(B) \propto \exp(-\frac{E_g(B)}{2k(T+T^*)})$ .

Here,  $kT^*$  accounts the kinetic energy window of charge carriers defined by  $eV_b/2$ . As seen in Fig.2 (left panel), an excellent agreement between experiments and simulation is obtained for the 90-aGNR energy gap with  $kT^* \approx 21 \pm 2\text{meV}$ , which is consistent with the 50mV experimental  $V_b$ . We thus conclude that if the sequence of the vHs for an aGNR of type 3m appears as the most likely fingerprint of the  $G(V_g)$  modulations at zero field, the agreement is further reinforced by the large positive MC.

*Transport simulations.*—To deepen the understanding of the large positive magnetoconductance signal, we perform tight-binding transport simulations using the Green functions formalism [20]. Three different types of disorders are considered: namely the Anderson disorder (with on-site energies varying at random in the range  $[-w/2, w/2]$  and  $w = 2\text{eV}$ ); the edge roughness with a 5% of removed carbon atoms on the six outer chains at each edge; and randomly dispersed impurities described by a long range Gaussian potential with a density  $1.15 \times 10^{16}\text{m}^{-2}$  (spatial range  $\xi = 1\text{nm}$ , maximum strength in the range  $[-u/2, u/2]$  with  $u = 2\text{eV}$ ). These disorders are well representative of the possible scattering sources considered in the literature [10–12]. In particular, edge roughness seems an unavoidable feature of nanoribbons, even when chemically derived; whereas impurities with long-range potential mimic screened charged ions trapped in the oxide. Finally Anderson disorder qualitatively reproduces the presence of impurities on the surface of the GNR. Transport calculations are performed at finite temperature  $T=80\text{K}$  and for a drain-source bias  $V_b = 50\text{mV}$ . The contribution of a contact resistance of  $10\text{k}\Omega$  in the ON-state of the current flow is also included [4].

Figure 3 shows the computed magnetoconductance profiles (at several gate voltages) for each type of disorder. First, it is clear that the use of the Anderson disorder seems inappropriate to describe the experimental magnetofingerprints. The conductance is indeed weakly sensitive to the magnetic field (only effective at low  $V_g \leq -5\text{V}$ ), and this behavior hardly changes with further modulation of the disorder strength ( $w$ ) (not shown here). In contrast, a huge positive MC is observed at low  $V_g$  (where only a single conductive channel is active) for the case of edge roughness. When two or three channels are available for conduction ( $-15\text{V} < V_g \leq -5\text{V}$ ), the MC displays however a more fluctuating trend, but becomes again positive at higher gate voltages (see  $V_g = -25\text{V}$ ). This partially reproduces the general trend of the measured MC, suggesting that edge roughness can partly account for disorder effects but does not fully dominate the scattering processes. Finally, Gaussian disorder qualitatively reproduces the experimental trend for all  $V_g$ . As in experiments, the conductance increases with gate voltage and the MC is positive at almost any magnetic field and  $V_g$  values. A more quantitative agreement between

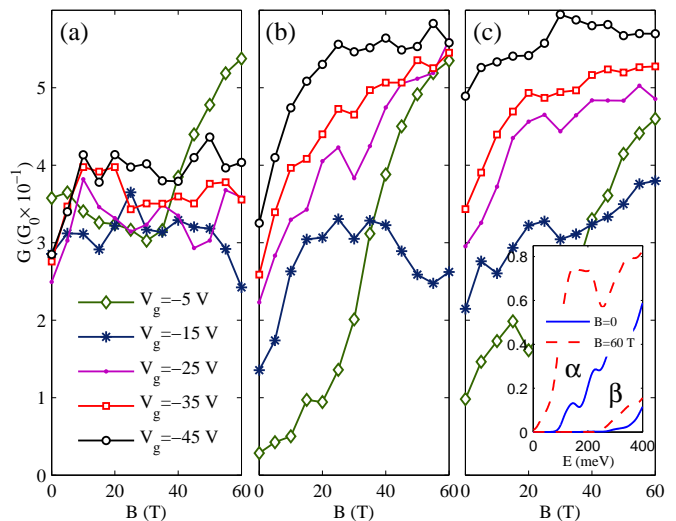


FIG. 3: (color online) Magnetoconductance for the 90-aGNR at different  $V_g$  with (a) Anderson disorder, (b) edge roughness and (c) Gaussian impurities. Inset of (c):  $\alpha$  and  $\beta$  transmission factors denote the contributions of the first channel and the higher bands at zero field and 60 T.

simulated and measured conductance data can only be achieved by considering a Gaussian disorder superimposed to an ultra-smooth roughness at the edges [15].

The positive MC behavior obtained for Gaussian impurities (or edge disorder) can be further rationalized by discussing and visualizing the magnetic edge states that develop in the GNR in the high magnetic field limit. These field-induced edge states have been already discussed in the context of quantum wires [21]. Due to the broken time-reversal symmetry, edge channels on the upper edge are created and convey current in opposite direction than the channels at the lower edge. If disorder is not strong enough, the spatial separation between the channels induced by the high magnetic field provokes a strong suppression of backscattering (and positive magnetoconductance). Figure 4 images the spectral current distribution at the energy  $E = 200\text{meV}$  for several magnetic fields. At zero magnetic field (a), the current flow is weak (as well as related conductance). Increasing  $B$  magnifies the current density along the ribbon (Fig.4-b,c), but the presence of scatters limit the total current flow between source and drain. Figure 4(d) illustrates the partial backscattering along the lower edge (where electrons can only move from right to left) and partial transmission to the right contact along the upper edge (yellow arrows), when the current flow reaches a localized state. This effect is further reduced with the formation of fully developed magnetic edges at higher magnetic field (see (e) for  $B = 60\text{T}$ ) which further enhances the positive MC signal.

One notes that for the Anderson disorder, the homo-

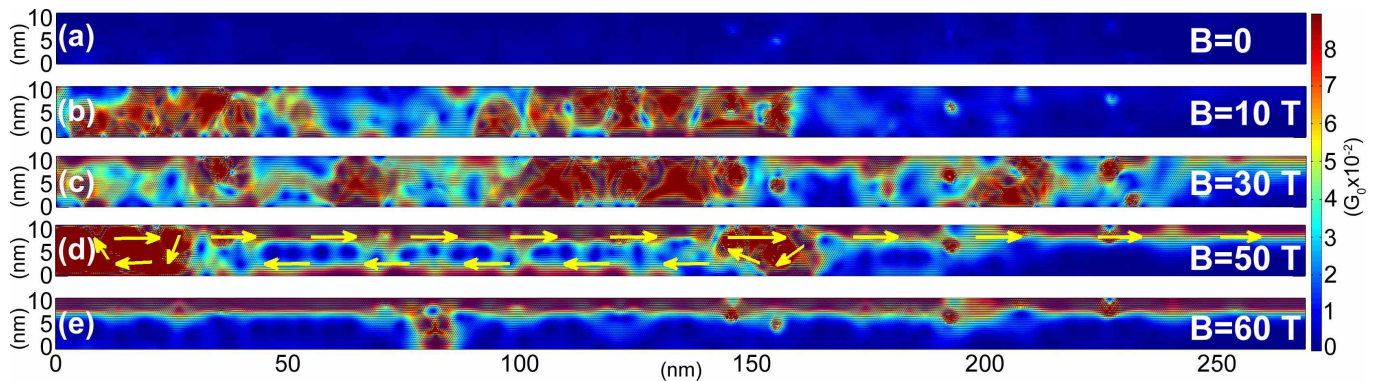


FIG. 4: (color online) Spectral current distribution at the energy  $E = 200\text{meV}$  for a 90-AGNR in the presence of Gaussian disorder only at (a)  $B=0$ , (b)  $B=10\text{ T}$ , (c)  $B=30\text{ T}$ , (d)  $B=50\text{ T}$ , (e)  $B=60\text{ T}$ . Charge flows from left to right.

geneous short-range scattering potential makes strongly difficult a spatial separation between the chiral channels, thus prohibiting the predominance of magnetic edge channels. In contrast, the mechanism is efficient on the first conductive channel when bulk disorder is absent (edge roughness) or weak and long-range scattering potential prevails. In this case, intraband scattering (within the first energy band) is partially suppressed and the conductance increases as the magnetic channels are pushed to the edges. A detailed analysis disentangles the contribution of the first channel from the higher subbands (represented by the  $\alpha$  and  $\beta$  factors, respectively [15]). For a Gaussian disorder,  $\alpha \gg \beta$  (Fig.3c-inset), so the first channel dominates transport and its magnetic field dependence. The long-range nature of the Gaussian potential markedly reduces the interband scattering and preserves the positive MC effect of the first channel well beyond the second vHs, as also observed experimentally. The higher channels are less active and do not show any marked positive MC. This is explained by the spatial enlargement of the magnetic edge states, which then come into contact more easily, due to the narrow width of the ribbon. Conversely, the short range nature of edge disorder favours enhanced interband scattering and mixing between channels, as evident from Fig.3b, where the positive MC is reduced when the second and third subbands start to be involved at  $V_g \simeq -10\text{ V}$ .

*Conclusion.*-In large magnetic field, charge transport properties in chemically derived graphene nanoribbons can be tuned by the formation of magnetic edge states. The resulting positive magnetoconductance fingerprint obtained experimentally has been further satisfactorily reproduced by quantum simulations, pinpointing the likely contribution of both charged impurities and smooth edge roughness.

Part of this work has been supported by Euro-MagNET, EU contract n° 228043. S.R. acknowledges the ANR/P3N2009 (project NANOSIM\_GRAPHENE n° ANR-09-NANO-016-01). H.D acknowledges funding

from Office of Naval Research (ONR) and Intel.

- 
- [1] A.K. Geim and K. Novoselov, *Nature Mater* **6**, 183 (2007).
  - [2] M.Y. Han *et al.*, *Phys. Rev. Lett.* **98**, 206805 (2007).
  - [3] G. Liang *et al.*, *IEEE Trans. Elec Dev.* **54**, 677 (2007).
  - [4] X. Wang *et al.*, *Phys. Rev. Lett.* **100**, 206803 (2008).
  - [5] Y-M. Lin *et al.*, *Phys. Rev. B* **78**, 161409(R) (2008).
  - [6] Y-W Son, M.L. Cohen, S.G. Louie, *Phys. Rev. Lett.* **97**, 216803 (2006).
  - [7] C. Stampfer *et al.*, *Phys. Rev. Lett.* **102**, 056403 (2009).
  - [8] M. Y. Han, J. C. Brant and Ph. Kim, *Phys. Rev. Lett.* **104**, 056801, (2010).
  - [9] P. Gallagher, K. Todd, and D. Goldhaber-Gordon, arXiv:0909.3886.
  - [10] D.A. Areshkin, D. Gunlycke and C.T. White, *Nano Lett.* **7**, 204 (2007). M. Evaldsson *et al.*, *Phys. Rev. B* **78**, 161407(R) (2008). T.C. Li and S.-P. Lu, *Phys. Rev. B* **77**, 085408 (2008). E.R. Mucciolo, A.H. Casto Neto and C. H. Lewenkopf, *Phys. Rev. B* **79**, 075407 (2009). D. Querlioz *et al.*, *Appl. Phys. Lett.* **92**, 042108 (2008). M. Yamamoto, Y. Takane and K. Wakabayashi, *Phys. Rev. B* **79**, 125421 (2009). A. Cresti *et al.*, *Nano Res.* **1**, 361 (2008). P. Zhao *et al.*, *Nano Res.* **1**, 395 (2008).
  - [11] S. Ihnatsenka and G. Kirczenow, *Phys. Rev. B* **80**, 201407(R)(2009)
  - [12] M.I Katsnelson and A.K Geim, *Phil. Trans. R. Soc. A* **366**, 195 (2008).
  - [13] K. Novoselov *et al.*, *Nature Phys.* **2**, 177 (2006). X. Wu *et al.*, *Phys. Rev. Lett.* **98**, 136801 (2007).
  - [14] X. Li *et al.*, *Science* **319**, 1229 (2008).
  - [15] See EPAPS Documents for supplementary material.
  - [16] F.V. Tikhonenko *et al.*, *Phys. Rev. Lett.* **100**, 056802 (2008).
  - [17] S. Cho and M.S. Fuhrer, *Phys. Rev. B* **77**, 081402(R) (2008).
  - [18] V.P. Gusynin and S.G. Girvin, *Phys. Rev. Lett.* **71**, 125124 (2005).
  - [19] T.S. Li *et al.*, *Phil. Mag.* **89**, 697 (2009).
  - [20] A. Cresti *et al.*, *Phys. Rev. B* **68**, 075306 (2003).
  - [21] A. Cresti, G. Grosso and G. Pastori Parravicini, *Phys. Rev. B* **77**, 115408 (2008).